ACS OMEGA

Article

Cite This: ACS Omega 2019, 4, 18392−18397

http://pubs.acs.org/journal/acsodf

Indirect-To-Direct Band Gap Transition of One-Dimensional V_2Se_9: Theoretical Study with Dispersion Energy Correction

Weon-Gyu Lee,[†] Sudong Chae,[‡] You Kyoung Chung,[†] Won-Sub Yoon,[§] Jae-Young Choi,*[,‡,∥] and Joonsuk Huh*[,†,∥]

[†]Department of Chemistry, [‡]School of Advanced Materials Science & Engineering, [§]Department of Energy Science, and [∥]SKKU Advanced Institute of Nanotechnology (SAINT), Sungkyunkwan University, Suwon 16419, Republic of Korea

Supporting Information

ABSTRACT: Recently, we synthesized a one-dimensional (1D) structure of V_2Se_9. The 1D V_2Se_9 resembles another 1D material, Nb_2Se_9, which is expected to have a direct band gap. To determine the potential applications of this material, we calculated the band structures of 1D and bulk V_2Se_9 using density functional theory by varying the number of chains and comparing their band structures and electronic properties with those of Nb_2Se_9. The results showed that a small number of V_2Se_9 chains have a direct band gap, whereas bulk V_2Se_9 possesses an indirect band gap, like Nb_2Se_9. We expect that V_2Se_9 nanowires with diameters less than ∼20 Å would have direct band gaps. This indirect-to-direct band gap transition could lead to potential optoelectronic applications for this 1D material because materials with direct band gaps can absorb photons without being disturbed by phonons.

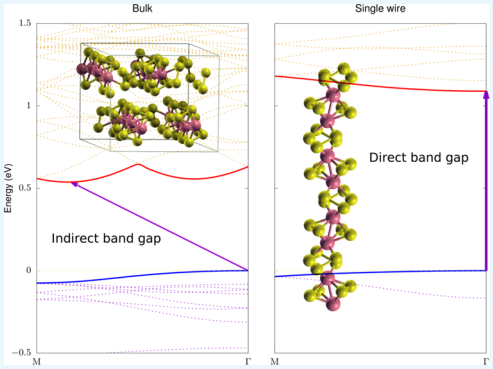

INTRODUCTION

The development of low-dimensional materials has launched different approaches to materials research for many promising applications.[1,2] Two-dimensional (2D) materials are composed of planar crystalline sheets stabilized by strong in-plane bonds and weak interlayer interactions. Because graphene was first separated from graphite, graphene-based applications in electronics, chemistry, and mechanics have been intensively studied due to graphene's superior physical properties (e.g., high charge carrier mobility and mechanical strength). However, graphene does not have a band gap and so is difficult to develop with transistors.[3,4] If graphene is finely patterned with narrow widths, a band gap can be formed.[3] Unfortunately, as the width of graphene decreases, the band gap increases, and the electron mobility sharply decreases. Other 2D materials with appropriate band gaps, including transition-metal dichalcogenides (TMDCs) and black phosphorus, have been introduced.[5−11] Similar to graphene, a dramatic reduction in charge carrier mobility due to edge scattering is inevitable after device manufacture.[12] The reduction of dimensionality also can influence the charge transfer, the structure of the crystal, spin property, or the charge carrier mobility in the metal nanowire system.[13−19]

Other types of one-dimensional (1D) materials, such as $Mo_6S_{9-x}I_x$, Sb_2Se_3, and VS_4, have been studied by several researchers.[20−26] Because they are formed by periodically stacking single-chain atomic crystals (SCACs) that have strong intrachain bonds with weak van der Waals (vdW) interchain interactions, these 1D materials are prepared by isolating SCACs from bulk crystals (similar to 2D materials). The structural characteristics of 1D materials result in a surface free from dangling bonds which hinder application of 2D materials.[27,28] However, it is difficult to clearly determine the crystal structure of $Mo_6S_{9-x}I_x$ because the positions of the sulfur and iodine ions coordinated to the central molybdenum ions may vary, even at the same stoichiometric composition. In addition, the thermodynamic properties of the ternary system (Mo−S−I) are not well known, which makes it difficult to understand the physical properties of the $Mo_6S_{9-x}I_x$ material. In addition, Sb_2Se_3 and VS_4 have not been reported experimentally as 1D atomic dispersions.

Very recently, other semiconducting 1D materials, such as Nb_2Se_9 and V_2Se_9, were reported to be successfully synthesized by solid-state reactions.[29,30] These materials can be separated as 1D nanowires up to a single-atomic chain size because of the weak vdW interactions between the selenium ions surrounding the inorganic chains. There are two approaches for preparing the nanowires: (i) mechanical exfoliation, which is similar to the conventional experimental set-ups used in 2D (e.g., graphene, boron nitride, and TMDCs) research,[31] and (ii) chemical exfoliation, which occurs by designing an appropriate solvent and dispersant.[32−34] Based on these two exfoliation methods, the bulk materials can be separated up to 1 nm in thickness [as experimentally confirmed by atomic force microscopy (AFM)]; the separated materials can be a single unit of the inorganic chain. In this report, we performed theoretical calculations to investigate the potential optoelec-

Received: August 17, 2019
Accepted: October 14, 2019
Published: October 25, 2019

DOI: 10.1021/acsomega.9b02655
ACS Omega 2019, 4, 18392−18397

tronic applications of V_2Se_9 chains after disintegration of bulk V_2Se_9 crystals into single V_2Se_9 chains.

The calculations showed that V_2Se_9 SCACs would have direct band gaps, whereas bulk V_2Se_9 would have an indirect band gap. As in Nb_2Se_9,[35] the band gap decreased by increasing the number of chains from 1.09 eV (single chain) to 0.54 eV (bulk). The band structures of single, double, triple, and septuple SCAC bundles were similar, but they were different from that of the bulk structure. We investigated the effects of vdW interchain interactions by adding the dispersion energy correction to the structural optimization. The dispersion energy decreased the band gaps but did not alter the indirect-to-direct band gap transition trend significantly, whereas the dispersion energy was important in predicting the direct band gap of the double-layer MoS_2.[36]

RESULTS AND DISCUSSION

Figure 1 shows the calculated band structures of bulk and few-chain systems, from the high symmetry point M to point Γ.

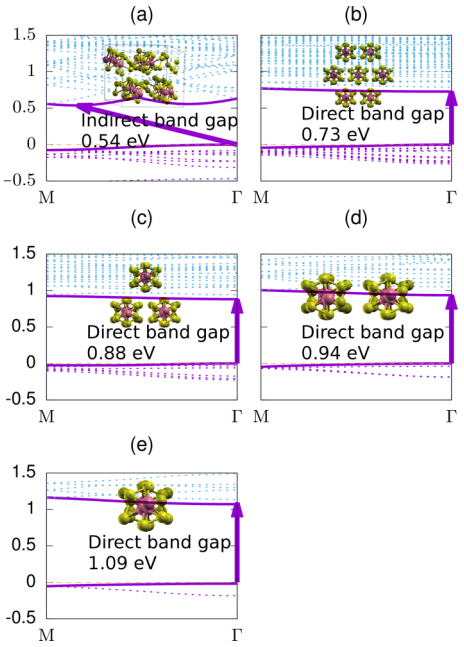

Figure 1. Part of band structures of (a) bulk, (b) 7-chain, (c) triple, (d) double, and (e) single SCAC(s) V_2Se_9 from point M to point Γ. The zero energy is shifted to the maximum energy of valence band. The structures are optimized by the Perdew−Burke−Ernzerhof (PBE) method with the DFT-D3 energy correction. Inset graphics represent the corresponding optimized structures of bulk and few-chain V_2Se_9.

Full band structures can be found in Supporting Information Figures S1−S5. Unlike 2D materials, a collection of 1D materials can have various arrangements. The lowest energy arrangements of the double and triple chains were chosen for the band structure calculation. Triangular arrangement of triple-chain V_2Se_9 is more stable than linear V_2Se_9, which implies that aggregation stabilizes the energy of V_2Se_9 SCACs. Thus, we calculated the band structure of hexagonally stacked septuple-chain bundles for seven chains. As Figure 1a presents, bulk V_2Se_9 had an indirect band gap of 0.54 eV from point Γ to a point (0.419, 0, 0.419) near M (0.5, 0, 0.5), designated as T. However, all 1D few-chain systems had direct band gaps that increased as the number of chains decreased. The maximum band gap was 1.09 eV in a single chain. Direct band gaps appeared at point Γ, a local minimum point in the conduction bands of few-chain systems but a local maximum point of the bulk structure. Point Γ was a local energy maximum in the few-chain system, unlike in the bulk system. The band energies of the conduction band at point Γ decreased as the number of chains increased in the few-chain systems. However, the conduction band at point T increased with the number of few-chain systems, whereas the conduction band energy of T in the bulk was minimal. This implies that the stacking effect on the energy at point Γ in the bulk is different from that in the few-chain systems. The partial orbital analysis showed that point Γ had larger contributions to p_z and d_{z^2} orbitals than did T (Figure S6). The different aspects of the conduction band near point M is the reason that bulk V_2Se_9 has an indirect band gap while the few-chain V_2Se_9 shows direct band gaps. The difference between the valence bands of bulk and few-chain systems is much smaller than the difference between the conduction bands. The number of chains has little influence on the valence band of few-chain and bulk V_2Se_9. The band structures of V_2Se_9 without the DFT-D3 dispersion energy correction are similar to the band structures with the DFT-D3, but the band gaps increase (Table S1).

We compared the band structures of V_2Se_9 with those of Nb_2Se_9. The band structures of Nb_2Se_9 with dispersion energy correction are shown in Figure S7. All few-chain systems have similar band structures in both V_2Se_9 and Nb_2Se_9. The valence bands of SCACs and bulk are also similar in both Nb_2Se_9 and in V_2Se_9. The contribution of selenium is greater than that of vanadium to the partial density of state both for the bulk and few-chain systems except the double chain (Figure S8). Screening of inner vanadium ions by outer selenium ions prevents the conduction band from being perturbed by other chains. The interactions between chains mainly change the characteristics related to selenium ions. However, the few V_2Se_9 chains have electronic bands with many valleys, whereas the few Nb_2Se_9 chains carry structureless bands.

All few-chain systems calculated previously have similar properties to a single chain. To determine the boundary between such few-chain systems and bulk systems, we plotted the changes in the band gap for a number of V_2Se_9 and Nb_2Se_9 chains, as in Figure 2. The band gap decreases as the number of chains increases, as does the change of the band gap. We expected that a decrease in the band gap (ΔE) by the number of chains (n) would approach the band gap in bulk V_2Se_9 at 0.54 eV and Nb_2Se_9 at 0.65 eV. We interpolated the tendency

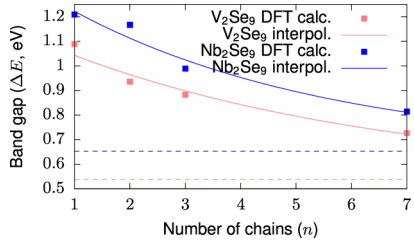

Figure 2. Band gap (ΔE) changes by the number of chains (n) of V_2Se_9 and Nb_2Se_9. calc. and interpol. abbreviate calculation and interpolation, respectively. As n increases, ΔE decreases to the bulk band gap of 0.54 eV in V_2Se_9 and 0.65 eV in Nb_2Se_9, as represented by dashed lines. We interpolated the band gap changes to exponential curves such that $\Delta E = 0.60\ e^{-0.17n} + 0.54$ for V_2Se_9 and $\Delta E = 0.70\ e^{-0.21n} + 0.65$ for Nb_2Se_9.

DOI: 10.1021/acsomega.9b02655
ACS Omega 2019, 4, 18392−18397

between ΔE and n as an exponential curve. From this interpolation, n satisfying $|\Delta E(n) - \Delta E_{bulk}| < 0.01$ eV, where ΔE_{bulk} is the band gap of the bulk system, is expected to be greater than 24 in V_2Se_9 and 20 in Nb_2Se_9. These numbers of chains can construct a triple-layer bundle with hexagonal stacking. The short interchain distance between two V_2Se_9 chains is 6.79 Å and the distance between two Nb_2Se_9 chains is 6.86 Å. Therefore, the shortest diameter of a triple-layer V_2Se_9 bundle is approximately 20.37 Å, and that of a triple-layer Nb_2Se_9 bundle is approximately 20.58 Å (supposing the cross-section of a bundle is an ellipse). The exponential function decays fast, and the number of chains enough to have a band gap similar to the bulk from exponential interpolation could be the lower bound. Thus, we believe that V_2Se_9 and Nb_2Se_9 SCACs thinner than about ∼20 Å would have the characteristics of single chains, such as a direct band gap. In the previous study of Nb_2Se_9 without dispersion correction, a value of 36 Å was suggested.[35]

The dispersion energy does not change the band gap transition trend in V_2Se_9 and Nb_2Se_9, although it is significant in 2D MoS_2. The reason is that such 1D materials have remarkably different conduction bands than the bulk material. With MoS_2, the 2D and 3D structures have a similar band structure to that of bulk MoS_2. The dispersion energy changes the size of the indirect and direct band gaps, while the positions of the band gaps are maintained. However, 1D few-chain V_2Se_9 and Nb_2Se_9 have significantly different band structures compared to those of 3D bulk structures. Unlike 2D TMDC, the effect of dispersion energy in these 1D material changes the positions of the indirect and direct band gaps. We expect that there would be bundles of V_2Se_9 and Nb_2Se_9 whose band structures have intermediate shape between that of a single chain and that of the bulk material, with the number of chains in these bundles more than seven.

Table 1 summarizes the characteristics of V_2Se_9 and Nb_2Se_9 calculated by PBE + DFT-D3. The band gap differences between the bulk and a single chain are similar in these materials. The size of the V_2Se_9 chain is 0.1 Å smaller than that of Nb_2Se_9, and the band gap of the bulk material and single chain of V_2Se_9 is 0.1 eV smaller than that of Nb_2Se_9. The physical properties related to the band gaps and the structures of chains in these two 1D materials are similar.

Table 1. Characteristics of V_2Se_9 and Nb_2Se_9 by PBE + DFT-D3 Theoretical Calculations

	V_2Se_9	Nb_2Se_9
crystal structure	$C2/c$	$P\bar{1}$
a (bulk, Å)	12.68	8.19
b (bulk, Å)	12.54	8.37
c (bulk, Å)	14.05	13.10
α (bulk, deg)	90	58.7
β (bulk, deg)	104.96	56.8
γ (bulk, deg)	90	92.5
number of chains ina cell	4	1
short interchain distance (bulk, Å)	6.79	6.86
long interchain distance (bulk, Å)	7.13	7.25
band gap of bulk (eV)	0.54, indirect	0.65, indirect
band gap of single chain (eV)	1.09, direct	1.21, direct
difference of band gaps of bulk and single chain (eV)	0.55	0.56
number of chains that makes the band gap near to bulk	24	21
short diameter of the chain bundle that makes band gap near to bulk (Å)	20.37	20.58

CONCLUSIONS

Using density functional theory (DFT) calculations, we found that 1−7 V_2Se_9 SCAC structures would have direct band gaps, whereas bulk V_2Se_9 would have an indirect band gap, like Nb_2Se_9 SCACs.[35] By interpolation, we predicted that a 1D V_2Se_9 chain with a diameter less than ∼ 20 Å would have a direct band gap. Additionally, we investigated the effect of vdW interactions between chains on the DFT-D3 energy correction. DFT-D3 correction maintained the structures of V_2Se_9 bulk and SCAC roughly, but the interchain distances were reduced. Band gaps of few chain systems decrease as the number of chains increases, with and without DFT-D3 correction, and finally approach the band gaps of the bulk structure. The band structures of SCACs with 1−7 chains are similar, and DFT-D3 optimization retains the band structures of V_2Se_9 systems qualitatively; however, the band gaps were reduced by DFT-D3 correction. The optimized structures and band gaps for various numbers of chains of V_2Se_9 showed similar characteristics to those of Nb_2Se_9. The dispersion energy does not change the band structure of these 1D materials, nor does it affect the indirect-to-direct band gap transition, unlike in the 2D material MoS_2.

This distinctive 1D material V_2Se_9 could be used in optoelectronic devices because it can absorb photon energy without being disturbed by phonons. The charge mobility calculation of 1D V_2Se_9 is needed to determine whether there are further applications for the field effect transistors that require a direct band gap and appropriately fast mobility, as with 2D MoS_2.[37,38] The spin property of this 1D material is also needed to be analyzed in future research. The 1D materials have higher surface-to-volume ratios and no dangling bonds, unlike the 2D materials; therefore, the 1D material V_2Se_9 described in this study seems to be a promising material in nanoelectronics.

STRUCTURES AND COMPUTATIONAL METHODS

Figure 3a shows the crystal structure of V_2Se_9, which is a periodic array of unit V_2Se_9 SCACs. Bulk V_2Se_9 crystals were prepared via the flux method using excess molten selenium as a solvent. When the V−Se liquid at 330 °C was cooled to room temperature, dark grey needles precipitated. Figure 3b shows a scanning electron microscopy (SEM) image of the V_2Se_9 needles prepared in this study. To demonstrate the characteristics of the chain-stacked structure of the V_2Se_9, the bulk V_2Se_9 crystal was cleaved using a conventional peeling method.[39] Figure 3c shows the AFM images of V_2Se_9 chains exfoliated from bulk V_2Se_9 crystals. The exfoliated chains had thicknesses of 1.1, 6.9, and 7.5 nm, indicating that single chains (1.1 nm) or bundles (6.9 and 7.5 nm) could be generated by mechanical exfoliation (Figure 3d). This result shows that weak vdW interactions among the chains in the bulk crystal results in V_2Se_9 crystals cleaved to V_2Se_9 chains, as in typical 2D materials.The bulk structure of V_2Se_9 has a monoclinic symmetry ($C2/c$). The unit of V_2Se_9 chain structures consists of four vanadium and 18 selenium ions, as in Nb_2Se_9. A V_4Se_{18} chain structure is composed of two V_2Se_4 octahedrons connected by Se_5; each octahedron faces the other octahedron (Figure 4a).[40] The relative coordinates of ions in the reference

DOI: 10.1021/acsomega.9b02655
ACS Omega 2019, 4, 18392−18397

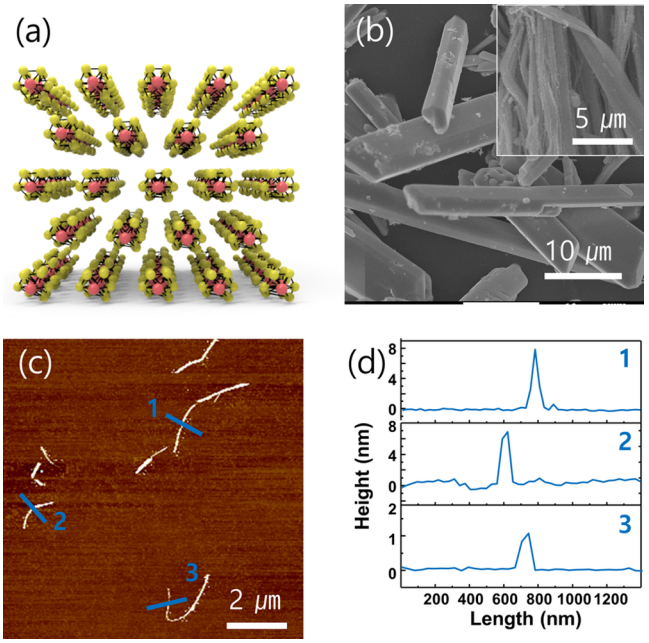

Figure 3. (a) Stick-and-ball crystal structure of V_2Se_9, where the red balls are vanadium and the yellow balls are selenium; (b) SEM images of the V_2Se_9 single crystal; (c) AFM image; and (d) height profiles of mechanically exfoliated V_2Se_9.

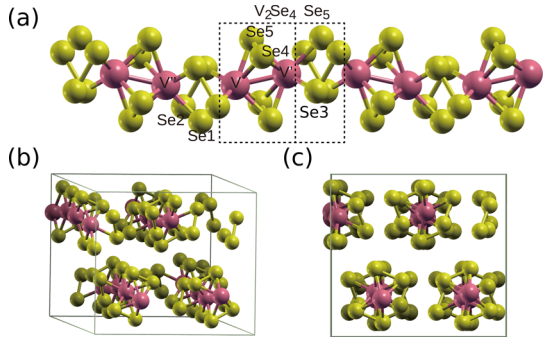

Figure 4. Views of V_2Se_9 single-lattice cells, which are rotated from the reference structure to direct the length of the chains to the [1 0 0] axis. (a) Two V_4Se_{18} chain units are shown, consisting of V_2Se_4 octahedrons and Se_5 connecting the octahedrons. The numbering of selenium and vanadium ions follows those of the reference.[40] An inclined view (b) and projected view (c) to the plane perpendicular to the length of chains are shown. A single cell has four chains. Two chains are stacked in the bottom of the unit cell as the first layer, and two chains are stacked on the top of the unit cell as the second layer. Two layers are shifted by a half-length between chains in each layer.

direct the chains to [1 0 1]. We rotated the lattice vectors to a set of ([1 0 1], [0 1 0], and [1 0 $\bar{1}$]). Then, 1D structures consisting of the number of finite chains could be constructed by repeating *k*-points into the *x*-axis in computational chemistry software. This rotated unit cell has three whole chain units and two half-chain units (Figure 4b,c). To validate the rotated frame, we calculated the band structures for the original and rotated lattice vector choices and compared the band gaps (see Figure S9).

We constructed few-chain systems that have single, double, triple, and septuple chain(s) by repeating the rotated unit cell to obtain the target chain arrangements and by removing redundancies. After the formation of the initial few SCAC systems, we optimized the structures of SCACs and bulk V_2Se_9. The calculation was performed using the projected augmented wave method[41,42] in the Vienna Ab-Initio Package (VASP).[43−46] Computational details are presented in the Supporting Information.

A theoretical calculation predicted that Nb_2Se_9 SCACs would have direct band gaps, bulk Nb_2Se_9 would have an indirect band gap, and the band gaps would increase as the number of chains decreased.[35] These phenomena are mainly caused by vdW interchain interactions. Previous studies of metal chalcogenides used only the generalized gradient approximation method,[35,47,48] which cannot properly describe vdW effects; therefore, further calculations were performed to incorporate vdW interactions.[36,49] We chose the DFT-D3 method, which introduces the dispersion energy correction proportional to $1/r^6$.[50,51] To investigate the effects of vdW interactions, we optimized the structures with and without the DFT-D3 correction and then compared the atomic structures and band structures of SCACs and bulk V_2Se_9. Indeed, when the dispersion correction was applied, the structure further approached the experimental reference structure (Table S2). The dispersion energy correction decreases the interchain distances of bulk and all SCAC V_2Se_9 and Nb_2Se_9 (Tables S3−S5 and Figures S10 and S11).

By looking at the electron localization function of the single chain and bulk V_2Se_9, we identified the bonding characters: the two Se−Se bondings in V_2Se_4 octahedron and two Se−Se bondings in Se_5 are covalent, and the Se−V bondings are ionic. Accordingly, we expect that the charge valence of V_2Se_9 would be $(V^{5+})_2(Se_2^{2-})_4Se^{2-}$. It implies that the system would be diamagnetic because there is no unpaired electron.

■ ASSOCIATED CONTENT

Supporting Information

The Supporting Information is available free of charge on the ACS Publications website at DOI: 10.1021/acsomega.9b02655.

Computational details, detailed atomic structures and band structures of V_2Se_9 and Nb_2Se_9, partial orbital analysis, and optimized structures of bulk and SCACs V_2Se_9 (PDF)

■ AUTHOR INFORMATION

Corresponding Authors

*E-mail: jy.choi@skku.edu (J.-Y.C.).
*E-mail: joonsukhuh@skku.edu (J.H.).

ORCID

Won-Sub Yoon: 0000-0002-6922-2088
Joonsuk Huh: 0000-0002-8792-5641

Author Contributions

W.-G.L. and S.C. contributed equally. The manuscript was written through contributions of all authors. All authors have given approval to the final version of the manuscript.

Notes

The authors declare no competing financial interest.

■ ACKNOWLEDGMENTS

This work was supported by a grant from NRF funded by the Korea government (nos. NRF-2017R1A4A1015770 and 2017M3A7B8065561).

DOI: 10.1021/acsomega.9b02655
ACS Omega 2019, 4, 18392−18397

ABBREVIATIONS

2D, two-dimensional; TMDC, transition-metal dichalcogenide; 1D, one-dimensional; SCAC, single-chain atomic crystal; vdW, van der Waals; VASP, Vienna Ab-Initio Package

REFERENCES

(1) Novoselov, K. S.; Geim, A. K.; Morozov, S. V.; Jiang, D.; Katsnelson, M. I.; Grigorieva, I. V.; Dubonos, S. V.; Firsov, A. A. Two-dimensional gas of massless Dirac fermions in graphene. *Nature* **2005**, *438*, 197.

(2) Zhang, Y.; Tan, Y.-W.; Stormer, H. L.; Kim, P. Experimental observation of the quantum Hall effect and Berry's phase in graphene. *Nature* **2005**, *438*, 201.

(3) Son, Y.-W.; Cohen, M. L.; Louie, S. G. Half-metallic graphene nanoribbons. *Nature* **2006**, *444*, 347−349.

(4) Avouris, P.; Chen, Z.; Perebeinos, V. Carbon-based electronics. *Nat. Nanotechnol.* **2007**, *2*, 605−615.

(5) Radisavljevic, B.; Radenovic, A.; Brivio, J.; Giacometti, V.; Kis, A. Single-layer MoS_2 transistors. *Nat. Nanotechnol.* **2011**, *6*, 147−150.

(6) Qiao, J.; Kong, X.; Hu, Z. X.; Yang, F.; Ji, W. High-mobility transport anisotropy and linear dichroism in few-layer black phosphorus. *Nat. Commun.* **2014**, *5*, 4475.

(7) Castellanos-Gomez, A.; Vicarelli, L.; Prada, E.; Island, J. O.; Narasimha-Acharya, K. L.; Blanter, S. I.; Groenendijk, D. J.; Buscema, M.; Steele, G. A.; Alvarez, J. V.; Zandbergen, H. W.; Palacios, J. J.; Van Der Zant, H. S. J. Isolation and characterization of few-layer black phosphorus. *2D Mater.* **2014**, *1*, 025001.

(8) Mayorov, A. S.; Gorbachev, R. V.; Morozov, S. V.; Britnell, L.; Jalil, R.; Ponomarenko, L. A.; Blake, P.; Novoselov, K. S.; Watanabe, K.; Taniguchi, T.; Geim, A. K. Micrometer-scale ballistic transport in encapsulated graphene at room temperature. *Nano Lett.* **2011**, *11*, 2396−2399.

(9) Feng, Q.; Liu, H.; Zhu, M.; Shang, J.; Liu, D.; Cui, X.; Shen, D.; Kou, L.; Mao, D.; Zheng, J.; Li, C.; Zhang, J.; Xu, H.; Zhao, J. Electrostatic Functionalization and Passivation of Water-Exfoliated Few-Layer Black Phosphorus by Poly Dimethyldiallyl Ammonium Chloride and Its Ultrafast Laser Application. *ACS Appl. Mater. Interfaces* **2018**, *10*, 9679−9687.

(10) Li, N.; Lee, G.; Jeong, Y. H.; Kim, K. S. Tailoring Electronic and Magnetic Properties of MoS_2 Nanotubes. *J. Phys. Chem. C* **2015**, *119*, 6405−6413.

(11) Sheehan, P. E.; Lieber, C. M. Friction between van der Waals Solids during Lattice Directed Sliding. *Nano Lett.* **2017**, *17*, 4116−4121.

(12) Schwierz, F. Graphene transistors. *Nat. Nanotechnol.* **2010**, *5*, 487−496.

(13) Cheng, D.; Kim, W. Y.; Min, S. K.; Nautiyal, T.; Kim, K. S. Magic structures and quantum conductance of [110] silver nanowires. *Phys. Rev. Lett.* **2006**, *96*, 096104.

(14) Nautiyal, T.; Youn, S. J.; Kim, K. S. Effect of dimensionality on the electronic structure of Cu, Ag, and Au. *Phys. Rev. B: Condens. Matter Mater. Phys.* **2003**, *68*, 033407.

(15) Choi, Y. C.; Lee, H. M.; Kim, W. Y.; Kwon, S. K.; Nautiyal, T.; Cheng, D.-Y.; Vishwanathan, K.; Kim, K. S. How can we make stable linear monoatomic chains? Gold-cesium binary subnanowires as an example of a charge-transfer-driven approach to alloying. *Phys. Rev. Lett.* **2007**, *98*, 076101.

(16) Bala, A.; Nautiyal, T.; Kim, K. S. Effect of dimensionality on transition-metal elements of groups 3-7. *Phys. Rev. B: Condens. Matter Mater. Phys.* **2006**, *74*, 174429.

(17) Nautiyal, T.; Rho, T. H.; Kim, K. S. Nanowires for spintronics: A study of transition-metal elements of groups 8-10. *Phys. Rev. B: Condens. Matter Mater. Phys.* **2004**, *69*, 193404.

(18) Woo, Y. K.; Nautiyal, T.; Suk, J. Y.; Kim, K. S. Anomalous behavior of mercury in one dimension: Density-functional calculations. *Phys. Rev. B: Condens. Matter Mater. Phys.* **2005**, *71*, 113104.

(19) Dua, P.; Lee, G.; Kim, K. S. Ferromagnetism in Monatomic Chains: Spin-Dependent Bandwidth Narrowing/Broadening. *J. Phys. Chem. C* **2017**, *121*, 20994−21000.

(20) Uplaznik, M.; Bercic, B.; Remskar, M.; Mihailovic, D. Quantum charge transport in $Mo_6S_3I_6$ molecular wire circuits. *Phys. Rev. B: Condens. Matter Mater. Phys.* **2009**, *80*, 085402.

(21) Sun, N.; McMullan, M.; Papakonstantinou, P.; Gao, H.; Zhang, X.; Mihailovic, D.; Li, M. Bioassembled Nanocircuits of $Mo_6S_{9-x}I_x$ Nanowires for Electrochemical Immunodetection of Estrone Hapten. *Anal. Chem.* **2008**, *80*, 3593−3597.

(22) Zhou, Y.; Wang, L.; Chen, S.; Qin, S.; Liu, X.; Chen, J.; Xue, D.-J.; Luo, M.; Cao, Y.; Cheng, Y.; Sargent, E. H.; Tang, J. Thin-film Sb_2Se_3 photovoltaics with oriented one-dimensional ribbons and benign grain boundaries. *Nat. Photonics* **2015**, *9*, 409.

(23) Wang, L.; Li, D.-B.; Li, K.; Chen, C.; Deng, H.-X.; Gao, L.; Zhao, Y.; Jiang, F.; Li, L.; Huang, F. Stable 6%-efficient Sb_2Se_3 solar cells with a ZnO buffer layer. *Nat. Energy* **2017**, *2*, 17046.

(24) Zhou, Y.; Li, Y.; Yang, J.; Tian, J.; Xu, H.; Yang, J.; Fan, W. Conductive polymer-coated VS_4 submicrospheres as advanced electrode materials in lithium-ion batteries. *ACS Appl. Mater. Interfaces* **2016**, *8*, 18797−18805.

(25) Lee, J. W.; Chae, S.; Oh, S.; Kim, S. H.; Choi, K. H.; Meeseepong, M.; Chang, J.; Kim, N.; Yong Ho Kim, K.; Lee, N.-E.; Lee, J. H.; Choi, J.-Y. Single-Chain Atomic Crystals as Extracellular Matrix-Mimicking Material with Exceptional Biocompatibility and Bioactivity. *Nano Lett.* **2018**, *18*, 7619−7627.

(26) Chung, Y. K.; Lee, W.-G.; Chae, S.; Choi, J.-Y.; Huh, J. Structural and electronic properties of $Mo_6S_3I_6$ nanowires by newly proposed theoretical compositional ordering. *Sci. Rep.* **2019**, *9*, 1222.

(27) Forti, S.; Emtsev, K. V.; Coletti, C.; Zakharov, A. A.; Riedl, C.; Starke, U. Large-area homogeneous quasifree standing epitaxial graphene on SiC(0001): Electronic and structural characterization. *Phys. Rev. B: Condens. Matter Mater. Phys.* **2011**, *84*, 125449.

(28) Rockett, A. Overview of Electronic Devices. *The Materials Science of Semiconductors*; Springer: New York, 2007; pp 73−140.

(29) Oh, S.; Chae, S.; Kim, B. J.; Siddiqa, A. J.; Choi, K. H.; Jang, W. S.; Lee, K. H.; Kim, H. Y.; Lee, D. K.; Kim, Y. M.; Yu, H. K.; Choi, J.-Y. Inorganic Molecular Chain Nb_2Se_9: Synthesis of Bulk Crystal and One-Atom-Thick Level Exfoliation. *Phys. Status Solidi RRL* **2018**, *12*, 1800451.

(30) Oh, S.; Chae, S.; Kim, B. J.; Choi, K. H.; Jang, W.-S.; Jang, J.; Hussain, Y.; Lee, D. K.; Kim, Y.-M.; Yu, H. K.; Choi, J.-Y. Synthesis of a one-dimensional atomic crystal of vanadium selenide (V_2Se_9). *RSC Adv.* **2018**, *8*, 33980−33984.

(31) Kim, B. J.; Jeong, B. J.; OH, S.; Chae, S.; Choi, K. H.; Nasir, T.; Lee, S. H.; Kim, K.-W.; Lim, H. K.; Choi, I. J.; Moon, J.-Y.; Yu, H. K.; Lee, J.-H.; Choi, J.-Y. Exfoliation and Characterization of V_2Se_9 Atomic Crystals. *Nanomaterials* **2018**, *8*, 737.

(32) Chae, S.; Siddiqa, A. J.; Oh, S.; Kim, B. J.; Choi, K. H.; Jang, W.-S.; Kim, Y.-M.; Yu, H. K.; Choi, J.-Y. Isolation of Nb_2Se_9 Molecular Chain from Bulk One-Dimensional Crystal by Liquid Exfoliation. *Nanomaterials* **2018**, *8*, 794.

(33) Chae, S.; Siddiqa, A. J.; Kim, B. J.; Oh, S.; Choi, K. H.; Lee, K. H.; Kim, H. Y.; Yu, H. K.; Choi, J.-Y. Isolation of inorganic molecular chains from rod-like bulk V_2Se_9 crystal by liquid exfoliation. *RSC Adv.* **2018**, *8*, 35348−35352.

(34) Chae, S.; Siddiqa, A. J.; Kim, B. J.; Oh, S.; Choi, K. H.; Kim, H. Y.; Lee, K. H.; Yu, H. K.; Choi, J.-Y. Design of dispersant structure for highly concentrated one-dimensional inorganic molecular chain from V_2Se_9 crystal. *Chem. Commun.* **2018**, *54*, 12190−12193.

(35) Lee, W.-G.; Chae, S.; Chung, Y. K.; Oh, S.; Choi, J.-Y.; Huh, J. New One-Dimensional Material Nb_2Se_9: Theoretical Prediction of Indirect to Direct Band Gap Transition Due to Dimensional Reduction. *Phys. Status Solidi RRL* **2019**, *13*, 1800517.

(36) Xiao, J.; Long, M.; Li, X.; Zhang, Q.; Xu, H.; Chan, K. S. Effects of van der Waals interaction and electric field on the electronic structure of bilayer MoS_2. *J. Phys.: Condens. Matter* **2014**, *26*, 405302.

DOI: 10.1021/acsomega.9b02655
ACS Omega 2019, 4, 18392−18397

(37) Mak, K. F.; Lee, C.; Hone, J.; Shan, J.; Heinz, T. F. Atomically Thin MoS_2: A New Direct-Gap Semiconductor. *Phys. Rev. Lett.* **2010**, *105*, 136805.
(38) Radisavljevic, B.; Radenovic, A.; Brivio, J.; Giacometti, V.; Kis, A. Single-layer MoS_2 transistors. *Nat. Nanotechnol.* **2011**, *6*, 147−150.
(39) Nicolosi, V.; Chhowalla, M.; Kanatzidis, M. G.; Strano, M. S.; Coleman, J. N. Liquid exfoliation of layered materials. *Science* **2013**, *340*, 1226419.
(40) Furuseth, S.; Klewe, B. Crystal Structure and Properties of V_2Se_9. *Acta Chem. Scand.* **1984**, *38a*, 467−471.
(41) Kresse, G.; Joubert, D. From ultrasoft pseudopotentials to the projector augmented-wave method. *Phys. Rev. B: Condens. Matter Mater. Phys.* **1999**, *59*, 1758−1775.
(42) Blöchl, P. E. Projector augmented-wave method. *Phys. Rev. B: Condens. Matter Mater. Phys.* **1994**, *50*, 17953−17979.
(43) Kresse, G.; Hafner, J. Ab initiomolecular dynamics for liquid metals. *Phys. Rev. B: Condens. Matter Mater. Phys.* **1993**, *47*, 558−561.
(44) Kresse, G.; Hafner, J. Ab initiomolecular-dynamics simulation of the liquid-metal-amorphous-semiconductor transition in germanium. *Phys. Rev. B: Condens. Matter Mater. Phys.* **1994**, *49*, 14251−14269.
(45) Kresse, G.; Furthmüller, J. Efficient iterative schemes forab initiototal-energy calculations using a plane-wave basis set. *Phys. Rev. B: Condens. Matter Mater. Phys.* **1996**, *54*, 11169−11186.
(46) Kresse, G.; Furthmüller, J. Efficiency of ab-initio total energy calculations for metals and semiconductors using a plane-wave basis set. *Comput. Mater. Sci.* **1996**, *6*, 15−50.
(47) Li, T.; Galli, G. Electronic properties of MoS_2 nanoparticles. *J. Phys. Chem. C* **2007**, *111*, 16192−16196.
(48) Lebègue, S.; Eriksson, O. Electronic structure of two-dimensional crystals from ab initio theory. *Phys. Rev. B: Condens. Matter Mater. Phys.* **2009**, *79*, 115409.
(49) Dybała, F.; Polak, M. P.; Kopaczek, J.; Scharoch, P.; Wu, K.; Tongay, S.; Kudrawiec, R. Pressure coefficients for direct optical transitions in MoS_2, $MoSe_2$, WS_2, and WSe_2 crystals and semiconductor to metal transitions. *Sci. Rep.* **2016**, *6*, 26663.
(50) Grimme, S.; Antony, J.; Ehrlich, S.; Krieg, H. A consistent and accurate ab initio parametrization of density functional dispersion correction (DFT-D) for the 94 elements H-Pu. *J. Chem. Phys.* **2010**, *132*, 154104.
(51) Grimme, S.; Ehrlich, S.; Goerigk, L. Effect of the damping function in dispersion corrected density functional theory. *J. Comput. Chem.* **2011**, *32*, 1456−1465.

DOI: 10.1021/acsomega.9b02655
ACS Omega 2019, 4, 18392−18397